

# Seismic Capacity Evaluation of an Instrumented Damaged School Building Strengthened with Acrylic Walls

**Jer-Fu Wang**

*Assistant Research Fellow, 921 Earthquake Museum of Taiwan, National Museum of Natural Science, Taichung City, Taiwan, R.O.C.*

**Chi-Chang Lin**

*Distinguished Professor, Department of Civil Engineering, National Chung Hsing University, Taichung City, Taiwan, R.O.C.*



## SUMMARY:

This paper evaluates the seismic capacity of the preserved Damaged South Classroom (DSC) building at the 921 Earthquake Museum of Taiwan (921EMT). The site of the 921EMT was a schoolyard before the 1999 Taiwan Chi-Chi Earthquake. For exhibition purposes, numerous acrylic walls were used to strengthen the DSC building, making it a unique retrofit case with seismic concerns. This study applies nonlinear static analysis and the capacity spectrum method to evaluate the seismic capacity of the existing structure. In contrast to the conventional approach in which some building parameters and response spectra are based on design codes, this study utilizes real dynamic parameters extracted from seismic measurements of the DSC building. Results show that the analyzed ground acceleration capacity is 0.5-0.6g in longitudinal direction and 0.8-1.0g in transverse direction. Although the weakness of the structure remains the same as before, its capacity is higher than the demand of the Taiwan seismic specification.

*Keywords:* Seismic capacity, pushover analysis, capacity spectrum method, structural health monitoring, vibration measurement.

## 1. GENERAL INSTRUCTIONS

On the 21st of September, 1999, movement along the Chelungpu Fault induced the Chi-Chi Earthquake with a magnitude of 7.3 on the Richter scale, creating a ground surface rupture nearly 100 kilometres long. This earthquake caused damage to tens of thousands of households. Among them, relative ground displacement through the athletic field, track, and classroom buildings at Kuangfu Junior High School in Wufeng Village, Taichung County astonished the public and became a hotspot at the time. To preserve this disaster site for commemoration and education, an earthquake museum named the “921 Earthquake Museum of Taiwan (921EMT)” was established and opened to the public in 2004. The Damaged South Classroom (DSC) is an exhibition building where visitors can observe its damage details closely. To preserve the building, four damaged columns were strengthened using traditional methods, and the sides of the other damaged columns were installed with acrylic walls (AWs) for the benefit of transparent display. However, acrylic is not a common material for structural components in buildings, and its reliability has not been verified in a real building case. To monitor the health conditions of the DSC building, a sensor array was deployed in 2010.

In this study, a procedure combining pushover analysis and the capacity spectrum method (ATC, 1996, Fajfar, 2000) was applied to evaluate the seismic capacity of the DSC building structure. A numerical model was established using ETABS software. The fundamental modal parameter was verified by comparing it with the identified modal parameters using the SRIM system identification technique (Juang, 1997; Lin et al., 2005, 2008), based on real acceleration measurements. Pushover analysis was then performed to obtain the capacity spectrum. The ground acceleration capacities in two horizontal directions were then calculated to represent the seismic capacity of the DSC building. The findings of this study will clarify the understanding of this special structure and provide useful information for the management of 921EMT.

## 2. OVERVIEW OF THE INSTRUMENTED DAMAGED SCHOOL BUILDING

Three damaged classroom buildings are preserved at the 921EMT. Two of were seriously damaged (totally collapsed in some portions or stories) because of the passage of the fault line. Museum visitors are not allowed to approach most of the remains because of safety concerns. The third damaged building is the DSC building. Although its base is almost intact, its columns are permanently deformed. The interior steel bars and cracks are exposed in many columns, making it a real example that can serve to educate people. Therefore, the DSC building was strengthened to allow visitors to pass through.

### 2.1. Building Description

The original DSC building, which is only five meters from the Chelungpu fault, encountered serious column damage along the corridor (in the x-direction) during the 1999 Chi-Chi Earthquake. The exhibition structure is a one-story building with a base size of 35m × 11m. Weight bearing, earthquake resistance, and damage display are the basic demands to this building. To achieve these goals, fourteen AWs were installed beside the damaged columns as the vertical and horizontal resisting elements, as shown in Figure 1.



**Figure 1.** Damaged South Classroom in 921 Earthquake Museum of Taiwan  
(Left: view from northwest; Right: AW retrofit)

### 2.2. Acrylic Wall

The AW is of box section composed of four acrylic plates (Figure 2). Each AW was installed between the beam and the ground with a steel-cement pedestal at each end joint. The weakest interface under lateral loads is the epoxy adhesive layer between the steel and the AW. The design shear strength of the adhesive is 100 kgf/cm<sup>2</sup>.

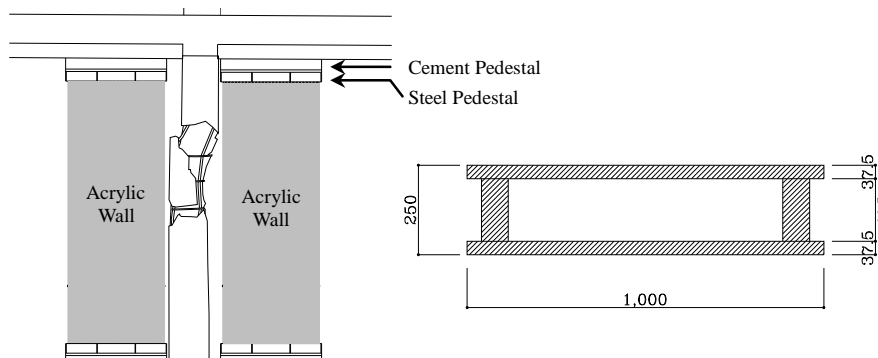


**Figure 2.** Configuration of AW retrofit

### 2.3. Sensor Array

The instrumentation project for the DSC building was completed in December 2010. Fifteen sensors including five uni-axial accelerometers at two locations on the ground floor, five uni-axial velocity sensors and one accelerometer at three locations on the roof, and four displacement sensors on four different AWs, were installed. Figure 3 presents the location, measured direction, and channel label of each sensor. Figure 4 shows the three sensor types. The velocity sensor on the roof is highly sensitive and can record ambient vibrations of high signal-to-noise ratio. Notably, each displacement transducer was installed horizontally to measure the gap distance between two wide acrylic plates. It is expected that the middle of the AWs will encounter contraction and expansion under loadings.

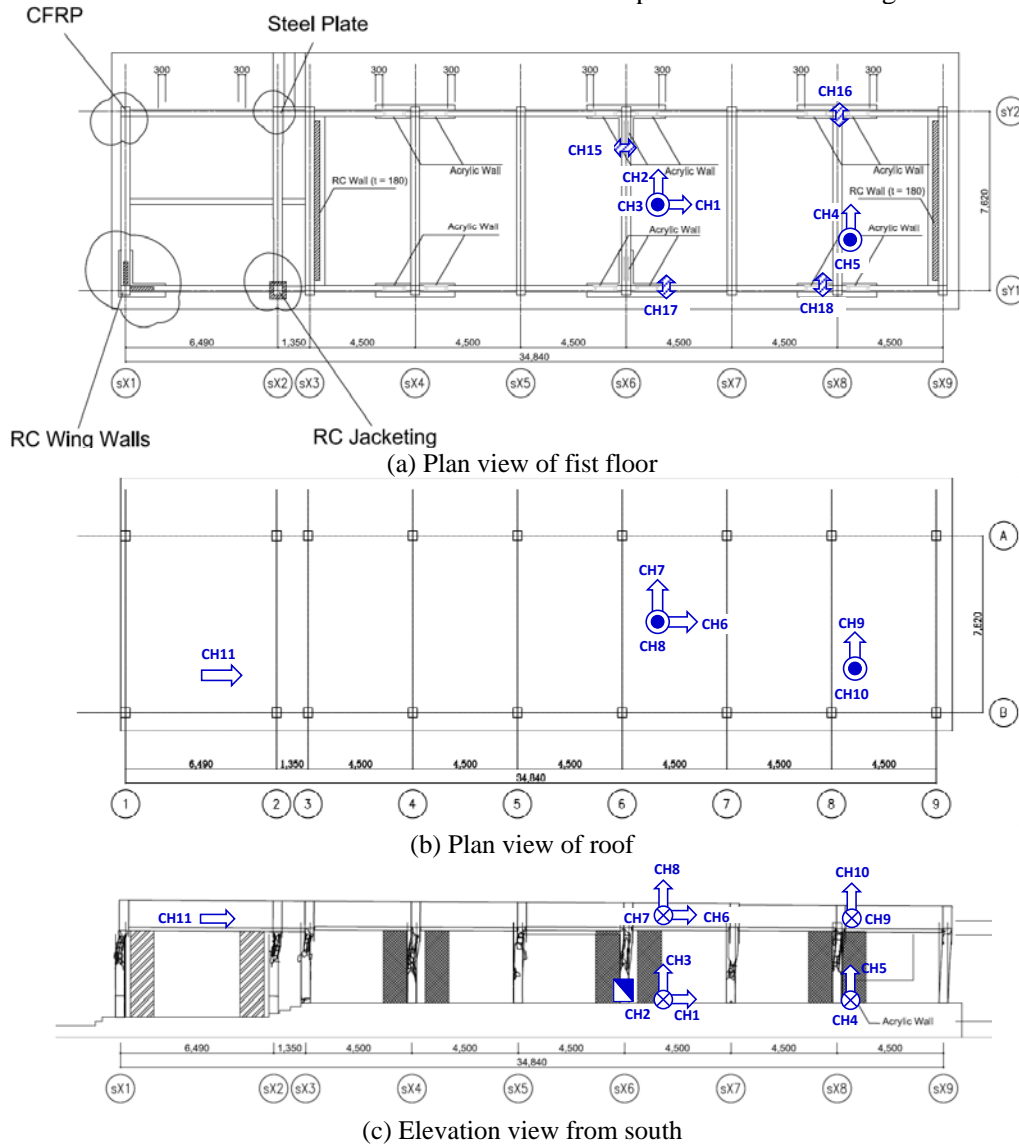


**Figure 3.** Sensor array deployment layout (measured positive direction:  $\Rightarrow$ : to the right;  $\odot$ : out from the paper;  $\otimes$ : into the paper;  $\Leftrightarrow$ : displacement transducer measured axis)

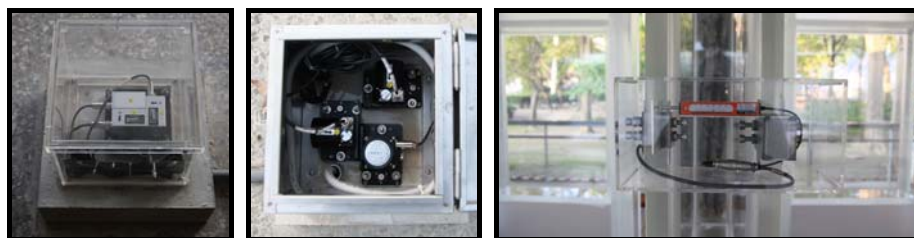


**Figure 4.** From left to right: accelerometers, velocity sensors, displacement transducer

### 3. DYNAMIC PROPERTY OF THE DSC BUILDING

#### 3.1. Loading Tests of AW

Before the manufacture of the AWs, a prototype with a steel connection at each end was designed and tested in a lab. Vertical load and lateral load were respectively applied, and the resulting force-displacement relationships are shown in Figure 5(a). Figure 5(b) shows the buckling of the AW. The behavior of the prototype is nearly linear and the shear strength is one-fifth of the axial strength. Some mechanical properties are presented in Table 1.

**Table 1.** Mechanical properties of the tested AW

Item	Physical parameters	Value	Remarks
Roof	A1.Length	3500 cm	measured
	A2.Width	1100 cm	measured
	A3.Thickness	25 cm	measured
	A4.Unit weight (concrete)	0.0024 kgf/cm <sup>3</sup>	theoretical
	A5.Weight	231000 kg	A1*A2*A3*A4
AW	B1.Axial load before damage	78000 kgf	tested
	B2.Axial displacement before damage	0.725 cm	tested
	B3.Lateral load before damage	15000 kgf	tested
	B4.Lateral displacement before damage	0.57cm	tested
	B5.Vertical stiffness	107586 kgf/cm	B1/B2
	B6.Lateral stiffness	26316 kgf/cm	B3/B4
	B7.Amount of AWs aligned in E-W direction	12	
	B8.Amount of AWs aligned in N-S direction	2	
	B9.Average vertical load of a single AW without considering other components	16500 kg	A5/(B7+B8)
	B10. Sectional area	1012.5 cm <sup>2</sup>	measured
	B11. Height	287 cm <sup>2</sup>	measured
	B12. Moment of inertia along strong axis	1.2 × 10 <sup>6</sup> cm <sup>4</sup>	calculated
	B13. Equivalent modulus of elasticity	43648 kgf/cm <sup>2</sup>	B6*B11 <sup>3</sup> /(12*B10)

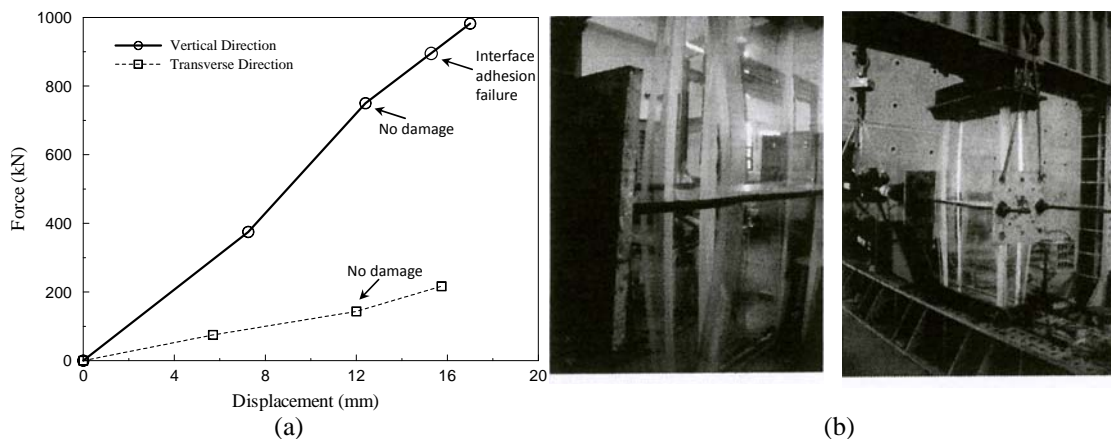


**Figure 5.** (a) Tested force-displacement relationship of the prototype AW; (b) Pictures of the test

#### 3.2. Numerical Model

In conducting pushover analysis, a numerical model of the DSC building was established using ETABS software. The damage of the original columns of the DSC building was modelled by setting the modulus of elasticity at half of the concrete material, based on a previous study of an in situ pushover test of a real school building (Jaung et al., 2008). Each acrylic wall was modelled as a line component; the section and material properties shown in Table 1.

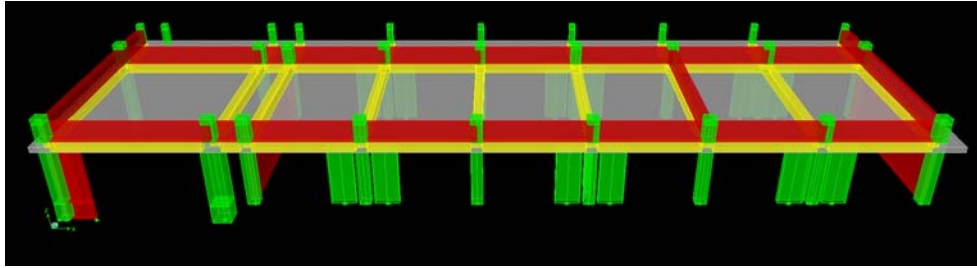


**Figure 6.** 3D view of the ETABS model of the DSC building

Figure 6 illustrates the ETABS model. The roof slab of the building was assigned as a rigid diaphragm to consider the compactness between the beam and the slab. By performing modal analysis, the first three modal frequencies and mode shapes were obtained, as shown in Table 2. Apparently, though the building has been strengthened, the softest axis is still the roof motion along the corridor (x-translation) as that of its undamaged state, but the first modal frequency is 13% higher than the fundamental frequency suggested by the Taiwan seismic code ( $1/0.07h^{3/4} = 1/0.07(2.87)^{3/4} = 6.48$  Hz), which means the stiffness is approximately 25% higher than a general building.

**Table 2.** Modal parameters of the DSC building by conducting ETABS modal analysis

Mode	Modal frequency	Mode shape	Mode shape chart	Mode shape description
1	7.46 Hz	$\begin{Bmatrix} 1.0000 \\ 0.0096 \\ 0.0000 \end{Bmatrix}$		x-translation dominated
2	21.2 Hz	$\begin{Bmatrix} -0.0179 \\ 1.0000 \\ -0.0004 \end{Bmatrix}$		y-translation and z-rotation coupled
3	27.8 Hz	$\begin{Bmatrix} 0.0292 \\ 0.0000 \\ 0.0021 \end{Bmatrix}$		z-rotation dominated

### 3.3. Vibration Measurement and System Identification

To verify the numerical model, the seismic measurements of the DSC building were collected and the modal parameters were identified using a system identification approach. In this study, the SRIM technique (Juang, 1997; Lin et al., 2005, 2008) was employed. The horizontal signals at ground level (CH01 and CH02) were set as inputs and the horizontal signals (CH06, CH07, and CH09) at roof level were set as outputs. Table 3 presents the identification results. The fundamental modal frequency (7.53 Hz) is quite close to that of the numerical model (7.46 Hz), supporting that the numerical model demonstrates acceptable accuracy. The range of the identified modal damping ratio is wide. The upper bound is from the largest-intensity event.

**Table 3.** Modal parameters of the DSC building based on seismic measurements (\*mean value)

Mode	Modal frequency*	Modal damping ratio (%)	Mode shape vector*	Mode shape description
1	7.53 Hz	0.4-6.24	$\{ 1.000 \ 0.010 \ 0.000 \}^T$	x-translation dominated
2	18.9 Hz	1.17-2.77	$\{ -0.053 \ 1.000 \ -0.001 \}^T$	y-translation and z-rotation coupled
3	23.8 Hz	1.46-4.8	$\{ 0.006 \ 1.000 \ 0.0004 \}^T$	y-translation and slight z-rotation coupled

## 4. SEISMIC CAPACITY EVALUATION

To evaluate the seismic capacity of the DSC building, nonlinear static analysis (pushover) and the capacity spectrum method based on the numerical model were performed as follows:

#### 4.1. Nonlinear hinges of structural components

In conducting nonlinear analysis, the ductility of structural components was considered. The nonlinear characteristic of a structural component was given by assigning nonlinear hinges according to its damage mechanism. Typically, the damage of a column can be dominated by bending or shearing. Two ends of a column may encounter bending-mode failure, whereas the other sections usually exhibit shear-mode failure. Therefore, in the ETABS model, a bending-type hinge was set at each end and a shear-type hinge was set in the middle of a column to determine the nonlinear characteristics. For the beams, only bending-type hinges at two ends were set because the beams are not of deep section. The lateral force-displacement relationships shown in Figure 7 were assumed in this study. Figure 8 shows the corresponding nonlinear hinge settings in the ETABS model (Chung et al., 2009).

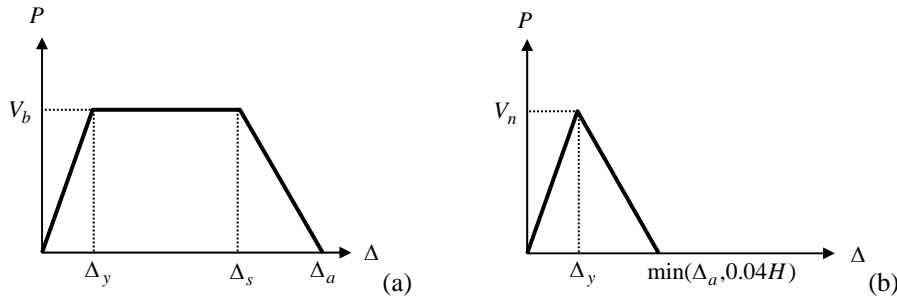


**Figure 7.** Lateral force-displacement curve of a nonlinear hinge with (a) bending-type or (b) shear-type damage for an RC column

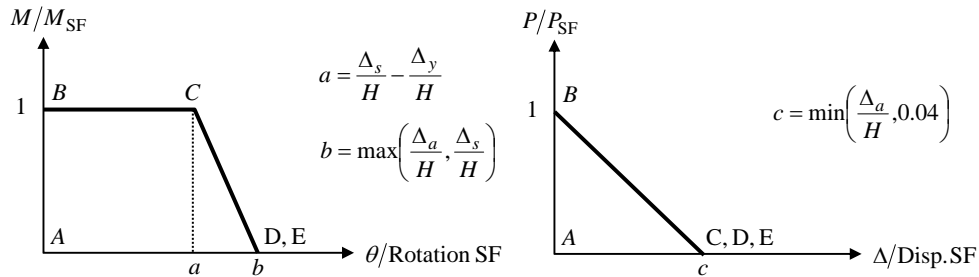


**Figure 8.** Nonlinear hinge property of (a) bending-type and (b) shear-type used for the RC columns

##### 4.1.1. RC Column

Figures 7 and 8 show that the displacements of yielding  $\Delta_y$ , shear failure  $\Delta_s$ , and axial failure  $\Delta_a$  are unknown. Chung et al. (2009) suggested that

$$\Delta_y = \frac{V_b}{k} \quad (4.1)$$

$$\frac{\Delta_s}{H} = \frac{3}{100} + 4\rho'' - \frac{1}{133} \frac{v_m}{\sqrt{f'_c}} - \frac{1}{40} \frac{P}{A_g f'_c} \geq \frac{1}{100} \quad (4.2)$$

$$\frac{\Delta_a}{H} = \frac{4}{100} \frac{1 + (\tan \theta)^2}{\tan \theta + P \frac{s}{A_{st} f_{yt} d_c \tan \theta}} \quad (4.3)$$

where  $V_b$  = the bending strength of the column with a double curvature ( $=2M_n/H$ , where  $M_n$  is the nominal bending strength of the section;  $H$  = the net height of the column);  $k$  = the lateral stiffness of a double-curvature column ( $=12(EI)_c/H^3$ );  $\rho'' = A_{st}/bs$  represents the volume ratio of a shear steel bar;  $A_{st}$  = the section area of a shear bar;  $b$  = the width of a column;  $s$  = the distance between shear bars;  $v_m = V_b/bd$  = shear stress;  $d$  = the effective depth of a column section;  $f'_c$  = the compressive stress of concrete;  $P$  = axial column force;  $A_g$  = the sectional area of a column;  $\theta$  = the angle between a shear crack and a horizontal line ( $=65^\circ$  but not more than  $\tan^{-1}(H/h)$  where  $h$  is the sectional height;  $f_{yt}$  = the yielding strength of a horizontal steel bar; and  $d_c$  = the depth of the concrete core.

#### 4.1.2. RC Columns with Steel Jacketing and CFRP Wrapping

For RC wing wall and RC jacketing retrofits, Eqs. (4.1) to (4.3) are still applied. For columns wrapped by other materials, the confinement effect has to be transformed into the equivalent horizontal bar distance before applying Eqs. (4.1) to (4.3). According to Lin et al. (2009), the confinement stress of horizontal bars can be obtained using

$$(f_l)_s = \frac{1}{2} k_e \left( \frac{A_{sx}}{s d_c} + \frac{A_{sy}}{s b_c} \right) f_{yh} \quad (4.4)$$

where  $k_e$  = the effective confinement coefficient (= 1.0 for steel jacketing and CFRP wrapping);  $A_{sx}$  = the section area in the x-direction;  $A_{sy}$  = the section area in the y-direction;  $b_c$  = the length of a horizontal bar the in x-direction;  $d_c$  = the length of a horizontal bar in the y-direction;  $f_{yh}$  = the yielding strength of a horizontal bar; and  $s$  = the distance between horizontal bars.

In addition, the confinement stress of any wrapping materials can be calculated using

$$(f_l)_r = \frac{2 f_{jd} t_f}{B} \quad (4.5)$$

where  $f_{jd}$  = the tensile strength of the wrapping material;  $t_f$  = the thickness of the wrapping material; and  $B$  = the width of a rectangular column. With  $(f_l)_s = (f_l)_r$ , the equivalent horizontal bar distance can be obtained using

$$s = \frac{k_e}{2} \left( \frac{A_{sx}}{d_c} + \frac{A_{sy}}{b_c} \right) \frac{f_{yh} B}{2 f_{jd} t_f} \quad (4.6)$$

#### 4.1.3. Setup of nonlinear hinges for four retrofitted columns

According to the previous equations, the nonlinear hinge parameters for ETABS settings of the four columns with different retrofit methods were obtained, as presented in Table 4.

**Table 4.** Nonlinear hinge property of the four columns with different retrofit methods

Retrofit method	Nonlinear hinge property						
	Bending-type				Shear-type		
	A	b	$M_n$ (kgf-cm)	$\Delta_y$ (cm)	c	$V_n$ (kgf)	$\Delta_y$ (cm)
RC jacketing	0.0387	0.0956	5577330	0.728	0.04	56753	1.189
Wing wall (x-dir.)	0.0498	0.0545	3829534	0.576	0.04	44129	1.066
Wing wall (y-dir.)	0.0247	0.0545	677733	2.726	0.04	14522	9.375
Steel jacketing	0.1040	0.1067	1814006	0.852	0.04	129069	9.734
CFRP wrapping	0.0701	0.0894	1008055	1.067	0.04	53002	9.001

#### 4.1.4. Setup of nonlinear hinges for AW

Because the failure of the AW is controlled by the shear strength at two ends, the test data discussed in Section 3.1 were used to establish the nonlinear hinge property. Here,  $c = 0.00565$ ,  $V_n = 18364$  kgf, and  $\Delta_y = 1.387$  cm.

## 4.2. Pushover Analysis

After setting the parameters of the nonlinear hinges, pushover analysis was performed. The force was applied at the mass center of the roof, and the observed displacement point was set at the same point. The obtained base shear versus roof displacement curve is shown in Figure 9(a). Figure 9(b) shows the state where the first nonlinear hinge on the AW was formed.

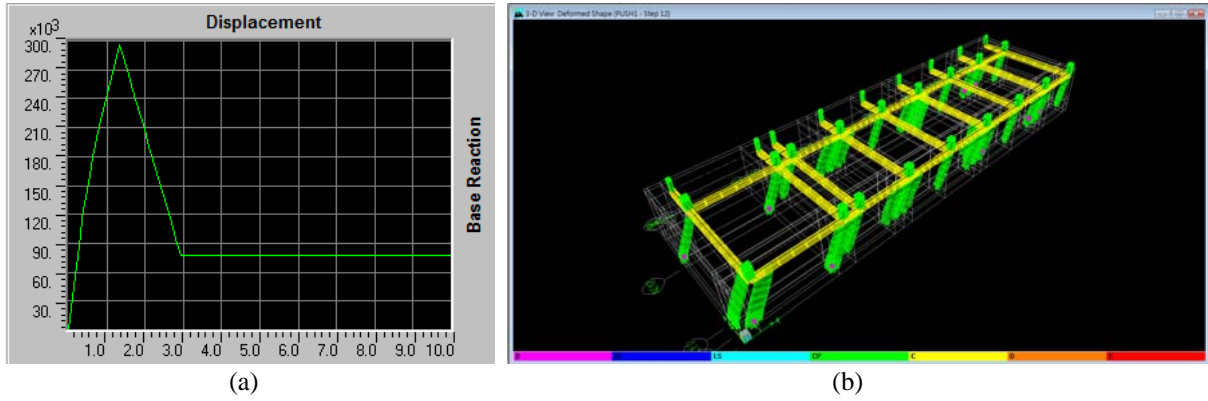


**Figure 9.** (a) Base shear versus roof displacement from the ETABS pushover analysis and (b) the locations of nonlinear hinges at the state of maximal shear

### 4.3. Seismic Capacity Analysis

#### 4.3.1 Design code basis

The  $V$ -versus- $\Delta_{roof}$  (base shear–roof displacement) curve (capacity curve) from the previous step can be transformed into an AD-format as a capacity spectrum curve using the following equations:

$$S_a = \frac{V}{W} \quad , \quad S_d = \Delta_{roof} \quad (4.7)$$

where  $V$  = maximal base shear;  $W$  = the weight of the building; and  $\Delta_{roof}$  = roof displacement. Using the AD-format capacity spectrum, the performance point  $(S_{a,p}, S_{d,p})$  can be determined. The ground acceleration capacity can then be obtained, based on the AT-format response spectrum. Conventionally, the elastic spectrum in the seismic design code is utilized. For the DSC building, the Taiwan design code was applied and the ground acceleration capacity can be represented by:

$$A_p = \begin{cases} S_{a,p} / \left[ 1 + \left( \frac{R_A}{B_s} - 1 \right) \frac{T_{eq}}{0.2T_0} \right] & \text{for } T_{eq} \leq 0.2T_0 \\ \frac{B_s}{R_A} S_{a,p} & \text{for } 0.2T_0 < T_{eq} \leq T_0 \\ \frac{B_s T_{eq}}{R_A T_0} S_{a,p} & \text{for } T_0 < T_{eq} \end{cases} \quad (4.8)$$

where  $T_0 = S_{D1} B_s / S_{DS} B_1$  represents the point between the short period and the mediate period, where  $S_{D1}$  = the horizontal acceleration spectral value at period of 1 sec;  $S_{DS}$  = the horizontal acceleration spectral value within short-period range;  $R_A$  = the ratio of the maximal spectral value to the zero-period spectral value with a 5% damping ratio in the seismic design code (=2.5 for this case);  $B_s$  and  $B_1$  are the damping modification coefficients, which are interpolated based on the equivalent damping ratio  $\beta_{eq}$ , as shown in Table 5;  $T_{eq} = 2\pi \sqrt{S_{d,p} / S_{a,p} g}$  = the equivalent period; and  $\beta_{eq}$  can be calculated using the following equation:

$$\beta_{eq} = \xi_0 + \kappa \frac{4A_e - 2S_{a,p} S_{d,p}}{\pi S_{a,p} S_{d,p}} \quad (4.9)$$

where  $\xi_0$  = the viscous damping ratio,  $\kappa$  is the damping modification factor used to describe the imperfection of the hysteresis loop. For RC structures,  $\kappa = 0.33$ .

**Table 5.** Damping modification coefficients for different values of equivalent damping ratio

$\beta_{eq}$	$B_s$	$B_1$
< 0.02	0.80	0.80
0.05	1.00	1.00
0.10	1.33	1.25
0.20	1.60	1.50
0.30	1.79	1.63
0.40	1.87	1.70
> 0.50	1.93	1.75

#### 4.3.2 Measurement basis

Section 4.3.1 presents the conventional approach to evaluate the ground acceleration capacity of a structure. For the DSC building, the response spectrum of a 5% damping ratio can be calculated based on the recorded time-history trace of the building site. Let  $PGA_m$  and  $S_{a,m}$  be the peak ground acceleration and spectral acceleration, respectively, at period  $T_{eq}$  along the measured direction in a seismic event. With the known  $S_{a,p}$  from Eq. (4.7), the ground acceleration capacity based on measurement, represented by  $A_p^m$ , can be calculated by

$$A_p^m = \frac{B_s}{(S_{a,m}/PGA_m)} S_{a,p} \quad (4.10)$$

#### 4.4. Results

The capacity curve in Figure 9 shows that before the base shear reaches the maximal value, the behavior of the DSC building is nearly linear; after that, the base shear is significantly reduced, which shows that almost all of the AWs encounter shear failure simultaneously and the low ductility property dominates the seismic capacity of the building. After the failure of AWs, the seismic resistance of the building is maintained solely by the four retrofitted columns.

Selecting the point with maximal  $S_a$  as the performance point; that is,  $S_{a,p} = 0.7349 g$  and  $S_{d,p} = 1.3272 cm$  and substituting them into Eq. (4.8) can obtain the ground acceleration capacities of  $A_{p,x} = 0.504 g$  in the x-direction and  $A_{p,y} = 1.023 g$  in the y-direction. The difference between these two values is consistent with the fact of two additional retrofit RC walls along the y-direction and the result of system identification.

In addition, this study collected the x- and y-direction ground acceleration time histories from 30 seismic events to create the response spectra of a 5% damping ratio for the DSC building site. The ground acceleration capacities along the two horizontal directions based on each event were then obtained using Eq. (4.10), as shown in Figure 10. The average  $A_{p,x}^m$  (0.560g; neglecting three outliers) and  $A_{p,y}^m$  (0.897g) in Figure 10 exhibit an approximately 11-12% difference from the seismic code-based ground acceleration capacities ( $A_{p,x} = 0.504 g$  and  $A_{p,y} = 1.023 g$ ). This implies that the seismic code spectrum shape can approximately describe the real site effect of the DSC building.

Considering the design code demand, the short period acceleration spectral value of the DSC building site in the Taiwan design code is,  $S_{DS} = 0.984$ . This building is a public building; hence, the importance factor is  $I = 1.25$ . The design ground acceleration is  $A_g = (0.4S_{DS})I = 0.492 g$ . This shows that the ground acceleration capacity ( $A_{p,x} = 0.504 g$  or  $A_{p,x}^m = 0.560 g$ ) of the DSC building satisfies the demand of seismic design specifications.

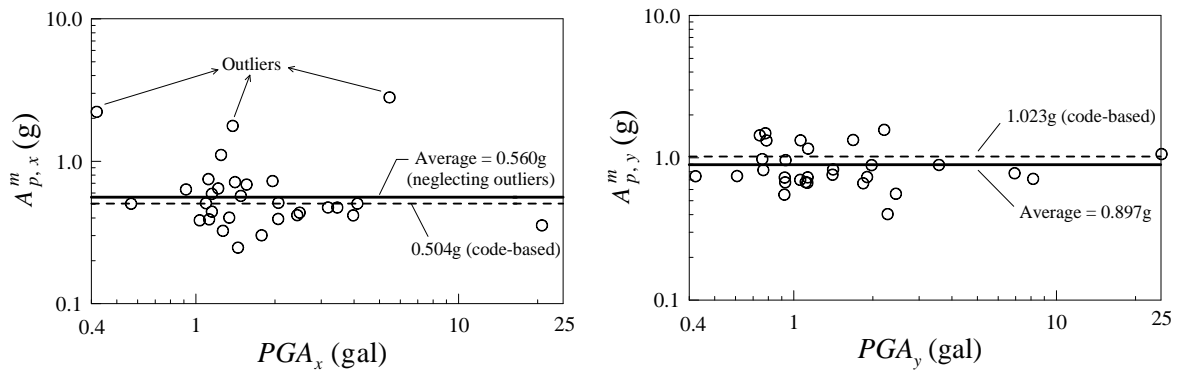


**Figure 10.** Ground acceleration capacities of the DSC building along the x- and y-directions, utilizing the ground acceleration measurements

## 5. CONCLUSIONS

This study evaluated the seismic capacity of the Damaged South Classroom building at the 921 Earthquake Museum of Taiwan. Numerous acrylic walls were used to strengthen the building. A procedure combining pushover analysis and the capacity spectrum method was applied to the numerical building model established using ETABS software. Analysis results show that the weakest direction is along the corridor of the DSC building with a ground acceleration capacity of approximately 0.5-0.6g, which satisfies the demand of the Taiwan seismic code. These results provide the museum manager with useful information for building retrofit decisions. Thus far, the sensor array continues to operate for the long-term monitoring of the behavior of the DSC building.

## ACKNOWLEDGEMENT

This work was supported by the National Science Council of the Republic of China under Grants NSC 99-2218-E-178 -001, NSC 100-2625-M-178-001, & NSC 100-2625-M-005-003. This support is greatly appreciated.

## REFERENCES

- ATC, (1996). Seismic evaluation and retrofit of concrete buildings. Vol. 1, *ATC 40, Applied Technology Council*, Redwood City, CA.
- Chung, L. L., Yeh, Y. K., Chien, W. Y., Hsiao, F. P., Shen, W. C., Chiou, T. C., Chow, T. K., Chao, Y. F., Yang, Y. S., Tu, Y. S., Chai, J. F., Hwang, S. J. and Sun, C. H. (2009). Technology handbook for seismic evaluation and retrofit of school buildings. *Report of National Center on Research of Earthquake Engineering, NCREE-09-023*.
- Fajfar, P. (2000). A nonlinear analysis method for performance based seismic design. *Earthquake Spectra*, **16(3)**: 573-592.
- Juang, W. C., Chiou, T. C., Hsiao, F. P., Tu, Y. H., Chien, W. Y., Yeh, Y. K., Chung, L. L. and Hwang, S. J. (2008). In-situ pushover test of school building structure in Sin-Chen Junior High School. *Report of National Center on Research of Earthquake Engineering, NCREE-08-008*.
- Juang, J. N. (1997). System realization using information matrix. *Journal of Guidance, Control, and Dynamics*, **21(3)**: 492-500.
- Lin, C. C., Wang, C. E., Wu, H. W. and Wang, J. F. (2005). On-line building damage assessment based on earthquake records. *Smart Materials and Structures*, **14(3)**: S137-S153.
- Lin, C. C., Wang, J. F. and Tsai, C. H. (2008). Dynamic parameter identifications for irregular buildings considering soil-structure interaction effects. *Earthquake Spectra*, **24(3)**: 641-666.
- Lin, M. L., Li, C. T., Chen, P. C., Tsai, K. C. and Wu, Y. H. (2009). Seismic retrofit of rectangular RC columns using CFRP wrapping and CFRP anchors. *Report of National Center on Research of Earthquake Engineering, NCREE-09-014*.